Geomechanics and Engineering, *Vol. 29, No. 4 (2022) 377-390*
https://doi.org/10.12989/gae.2022.29.4.377

Experimental study on rock-coal-rock composite structure with different crack characteristics

Tan Li*[1,2], Guangbo Chen[1] and Qinghai Li[2]

[1]*Institute of Mining and Coal, Inner Mongolia University of Science and Technology, Baotou 014010, China*
[2]*College of Energy and Mining Engineering, Shandong University of Science and Technology, Qingdao 266590, China*

(Received June 7, 2021, Revised March 2, 2022, Accepted March 29, 2022)

Abstract. The stability of the roof rock-coal pillar-floor rock composite structure is of great significance to coal mine safety production. The cracks existing in the composite structure seriously affect the stability of the roof rock-coal pillar-floor rock composite structure. The numerical simulation tests of rock-coal-rock composite structures with different crack characteristics were carried out to reveal the composite structures' mechanical properties and failure mechanisms. The test results show that the rock-coal-rock composite structure's peak stress and elastic modulus are directly proportional to the crack angle and inversely proportional to the crack length. The smaller the crack angle, the more branch cracks produced near the main control crack in the rock-coal-rock composite structure, and the larger the angle between the main control crack and the crack. The smaller the crack length, the larger the width of the crack zone. The impact energy index of the rock-coal-rock composite structure decreases first and then increases with the increase of crack length and increases with the increase of crack angle. The functional relationships between the different crack characteristics, peak stress, and impact energy index are determined based on the sensitivity analysis. The determination of the functional relationship can fully grasp the influence of the crack angle and the crack length on the peak stress and impact energy index of the coal-rock composite structure. The research results can provide a theoretical basis and guidance for preventing the instability and failure of the coal pillar-roof composite structure.

Keywords: crack characteristic; energy characteristic; mechanical property; rock-coal-rock composite structure; sensitivity analysis

1. Introduction

In order to ensure the safe and efficient mining of coal resources, a large number of coal pillars need to be left around the stope, such as strip coal pillars, section coal pillars, waterproof coal pillars, and fault-protected coal pillars (Frith and Reed 2018, Wang *et al.* 2019). These reserved coal pillars play the role of natural support, boundary, and isolation, and the stability of the combined system of the reserved coal pillars and its roof and floor determines the safety of the entire stope, overlying rock, and even the surface. If the rock-coal-rock composite system is destroyed and unstable, it will bring many disastrous consequences, ranging from damage to surface buildings to sudden "collapse" of the surface, resulting in heavy casualties and property losses (Li *et al.* 2021, Li *et al.* 2021, Thin *et al.* 1993, Wang *et al.* 2015, Xie *et al.* 2011).

The cracks with different characteristics existing in the composite structure seriously affect the stability of the rock-coal-rock composite structure. Therefore, studying the influence of different crack characteristics on the mechanical properties and stability of the composite structure of roof rock-coal pillar-floor rock is of great significance to ensure the safety of coal mine production (Wu *et al.* 2015, Bai *et al.* 2015, Zha *et al.* 2017, Yang *et al.* 2015).

At present, many experts and scholars have transformed the study of roof rock-coal pillar-floor rock into the study of rock-coal-rock composite structure, as shown in Fig. 1 (Wang *et al.* 2018). Ma *et al.* (2020) conducted uniaxial compression tests on rock-coal-rock sandwich composites with different coal thicknesses and discussed the influence of coal thickness on the energy characteristics of rock-coal-rock sandwich composites. Dou *et al.* (2006) used acoustic emission and electromagnetic radiation to monitor the coal-rock composite structure and considered that the greater the content and strength of the rock in the coal-rock composite structure, the more favorable the occurrence of rockburst. Zuo *et al.* (2011) used the triaxial compression tests of the coal-rock composite structure to study the influence of confining pressure strength on the peak strength, elastic modulus, and failure mode. Jiang *et al.* (2013) obtained the relationship between axial load and sliding form through the double-sided shear experimental model to study the occurrence condition, sliding type, and acoustic emission characteristics of the coal-rock composite structure. Antonio and Haitao (2015) obtained the closed-form solutions of singular stress and displacement fields at the tip of a single crack in transversely anisotropic saturated media with infinite pore elasticity. Sivakumar and Maji (2018) studied the crack initiation and propagation of cracked rock under uniaxial compression through laboratory experiments and subsequent numerical simulation. The change of crack

*Corresponding author, Ph.D.
E-mail: litan597@163.com

ISSN: 2005-307X (Print), 2092-6219 (Online)

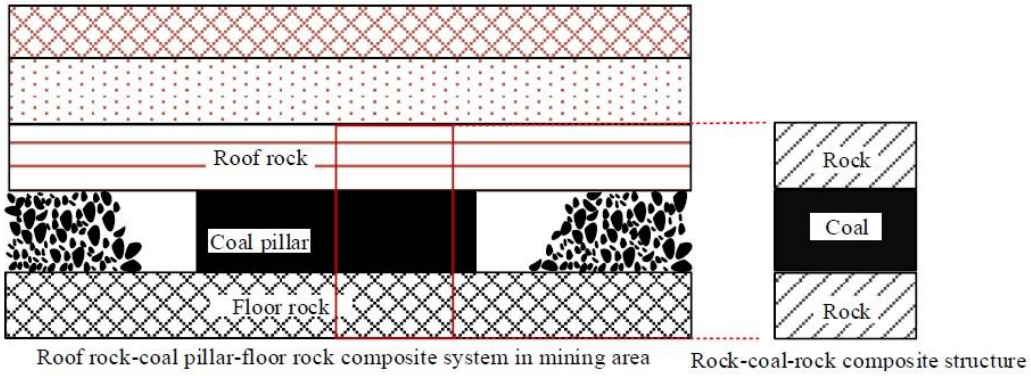

Fig. 1 Rock-coal-rock composite structure

initiation and peak stress with crack propagation mode was observed at different crack angles. Kurlenya and Mirenkov (2018) proposed a phenomenological theory to calculate the total displacement near the crack: tension is generated above the crack, and compression is generated below the crack. Kamran *et al.* (2015) considered that the geometric parameters calculated by mechanical properties could be used to judge the anisotropy and strength of the crack region reliably. Chen *et al.* (2019) performed uniaxial compression tests on sandstone-coal composite samples with acoustic emission (AE) device and digital video camera and analyzed the effects of pre-existing cracks in coal on composite strength, macroscopic failure initiation, and failure characteristics. Zhao *et al.* (2020) established an equivalent homogeneous model of coal-rock assembly and its stress state expression based on the principle of equivalent strain energy. The general compression-shear failure criterion of the equivalent model considering the bond strength of the coal and soft rock interface is derived.

Many experimental studies have shown that coal specimens are the most fragile part of the rock-coal-rock composite structure, which plays an important role in the mechanical properties and stability of the rock-coal-rock composite structure. Therefore, studying influence of different crack characteristics of the coal sample on the rock-coal-rock composite structure's mechanical properties and impact energy index can provide a theoretical basis for preventing the progressive instability of roof rock-coal pillar-roof rock composite structure and the failure of roadway surrounding rock. These research conclusions are important and valuable for understanding the crack mechanism of rock engineering in deep underground mining excavations.

2. Parameter selection and model establishment

2.1 Parameter selection

The coarse sandstone, mudstone, and coal samples used in the test were taken from Xin'an Coal Mine, Heilongjiang Province, China. The test system of this test mainly includes coal and rock CT scanning system, electro-hydraulic servo pressure control system, and DVC system, as shown in Fig. 2. During the test, the electro-hydraulic servo pressure control system and DVC system are synchronized to ensure that the system has the same time parameters. According to the measurement of uniaxial compressive strength in part 7 of "measurement methods for physical and mechanical properties of coal and rock," the uniaxial compression deformation test is carried out on the specimen, and the loading speed is 0.005 mm/s until the specimen is unstable.

PFC is a numerical model constructed by each rigid particle (3D) or disk (2D) with finite mass and defined surface (Liu *et al.* 2019, Dehghan and Mohammadi 2016). The software defines different types of contact models by calibrating parameters to complete the transfer of force and moment between internal particles, which is an effective method to achieve micromechanics. It has been widely used to study rock crack and cracks propagation (Zhou *et al.* 2017).

There are three contact modes between particles in PFC simulation software: pure friction model, contact bonding model, and parallel bonding model (Lisjak and Grasselli 2014). The parallel bonding model is selected in this paper mainly because the parallel bonding can transfer the force and the bending moment, which can better simulate the rock. In the parallel bond model, the normal stiffness mainly controls the Poisson's ratio, the tensile strength and cohesion of parallel mainly control the peak stress of the material. The effective modulus of parallel bonds mainly controls the elastic modulus of material (Filgueira *et al.* 2017, Hadjigeorgiou *et al.* 2008).

By modifying the micro-parameters, the numerical simulation results are very close to the mechanical properties obtained in the laboratory test, and it can be determined that the setting of related parameters meets the accuracy requirements of the simulation test. The CT scanning images and experiment results of coarse sandstone, mudstone, and coal samples are shown in Figs. 3-5.

The reasonable setting of micro-mechanical parameters directly determines the matching degree between numerical simulation and experiment results. The micro-mechanical parameters are obtained by constantly adjusting the micro-

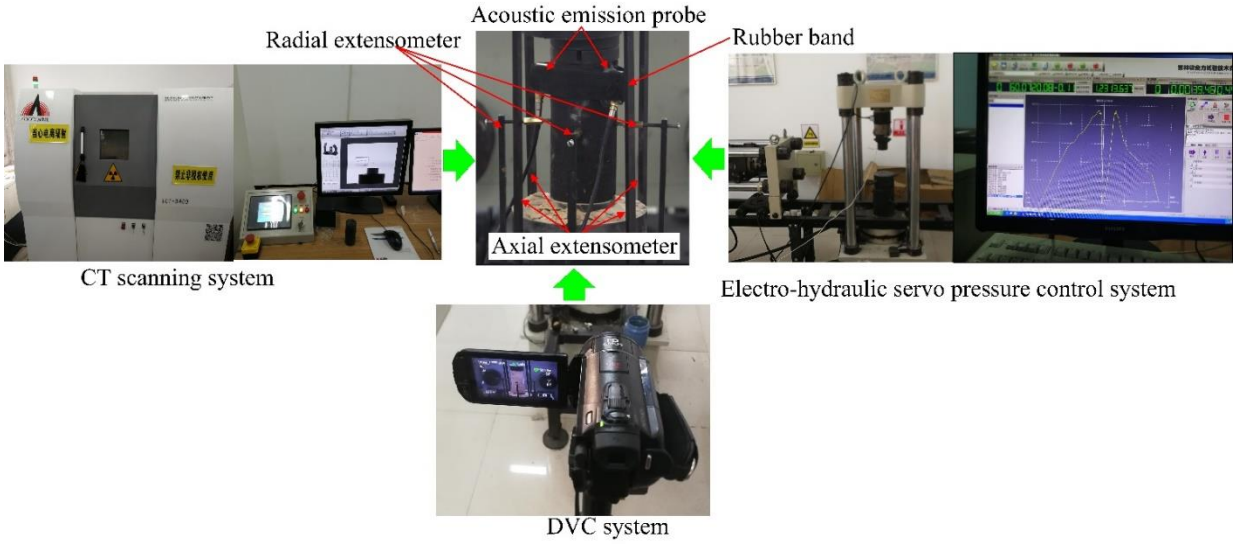

Fig. 2 Test system

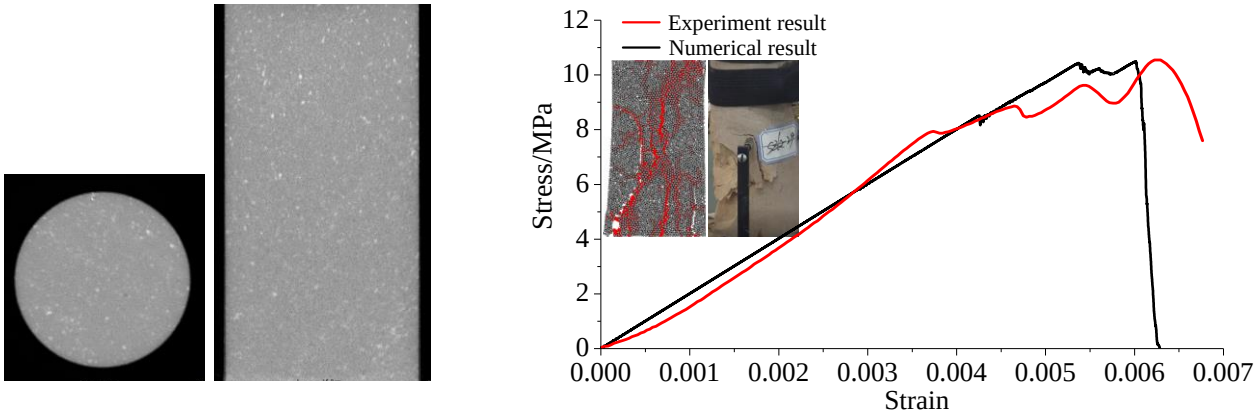

(a) CT image of coarse sandstone (b) Experiment results of coarse sandstone

Fig. 3 CT image and experiment results of coarse sandstone

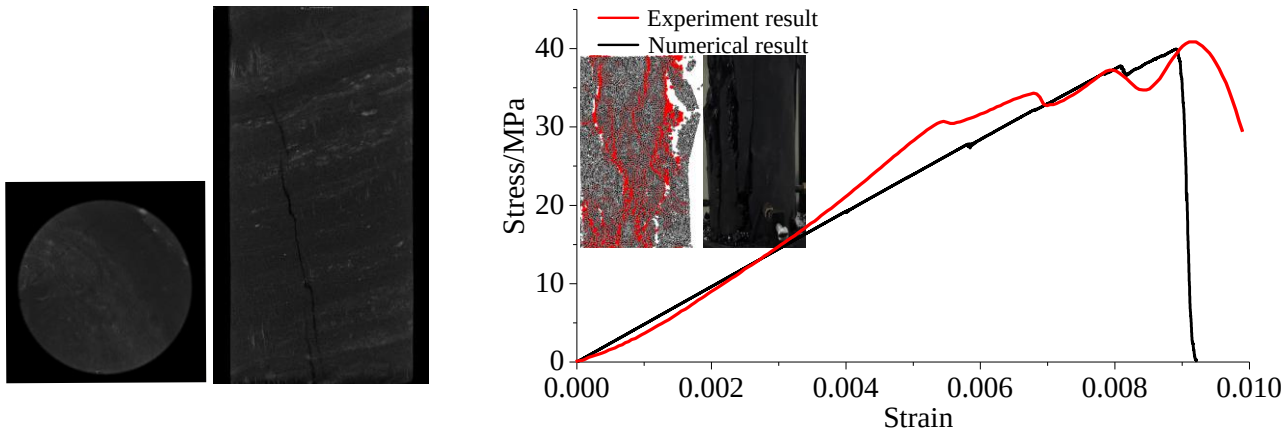

(a) CT image of coal (b) Experiment results of coal

Fig. 4 CT image and experiment results of coal

mechanical parameters according to the elastic modulus, Poisson's ratio, and macroscopic failure state of the rock specimens, to minimize the error between the simulation results and the experiment results.

It can be seen from the CT images that there are no obvious cracks in the coarse sandstone specimens and mudstone specimens, and there are obvious cracks in the coal specimens. Numerical simulation results of coarse

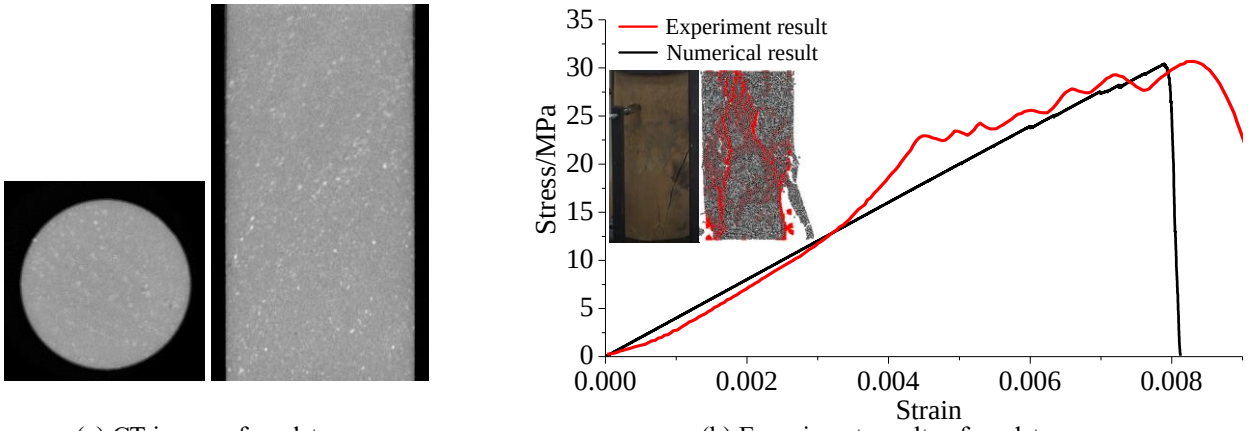

(a) CT image of mudstone (b) Experiment results of mudstone

Fig. 5 CT image and experiment results of mudstone

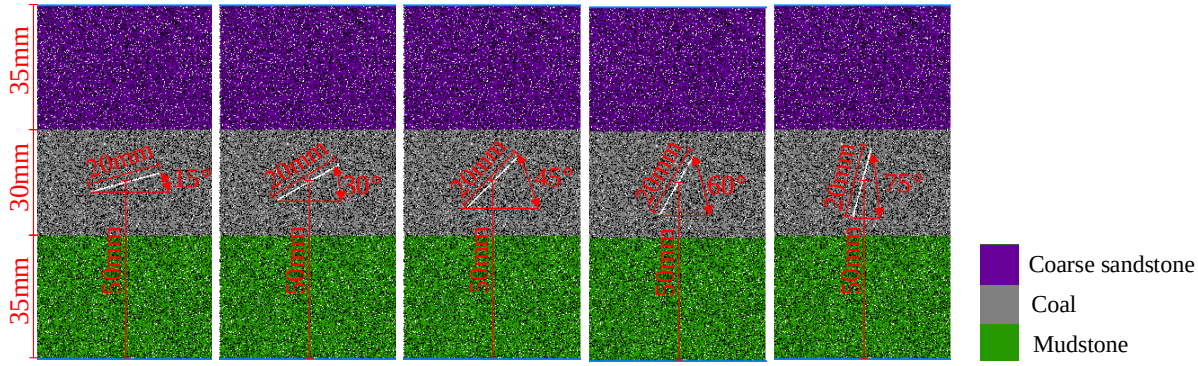

Fig. 6 Rock-coal-rock composite structure with different crack angles

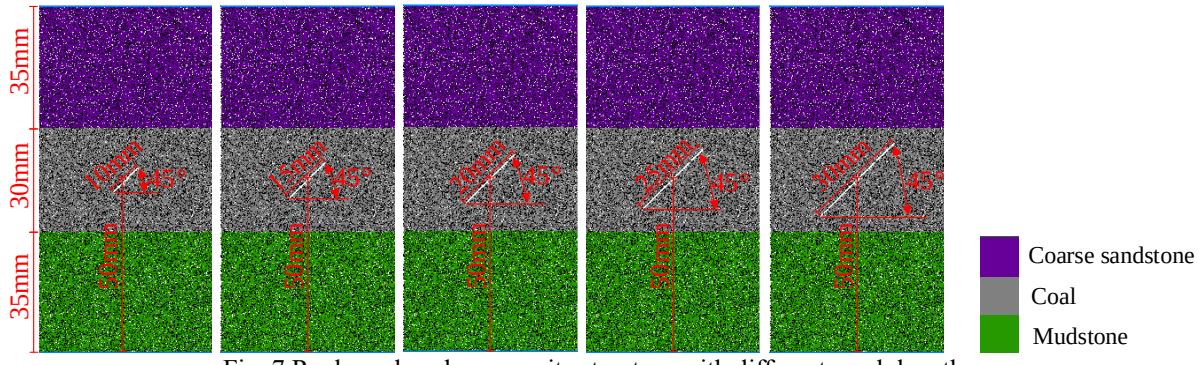

Fig. 7 Rock-coal-rock composite structure with different crack lengths

Table 1 The micro-mechanical parameters

Micro-mechanical parameters	Coal	Coarse sandstone	Mudstone
Particle density /(kg·m^{-3})	1830	2320	2580
Radius /mm	0.2~0.3	0.2~0.3	0.2~0.3
Friction coefficient	0.12	0.18	0.17
Contact modulus /GPa	4	12	10
Parallel bond modulus /GPa	4	13	11
Parallel bond normal / tangential strength /MPa	16	45	37
Parallel bond normal / tangential stiffness	2.5	3.2	2.9
The parallel bond radius value	1	1	1

sandstone, coal, and mudstone have similar failure patterns to the experimental results. Coarse sandstone specimens have fragmentation failure, coal specimens have a split failure, and mudstone specimens have large cracks at the bottom. The micro-mechanical parameters are shown in Table 1.

2.2 Model establishment

Many scholars have studied the stability of the rock-coal-rock composite structure and believe that the coal specimen is the weak part of the rock-coal-rock composite structure and the main factor determining the mechanical

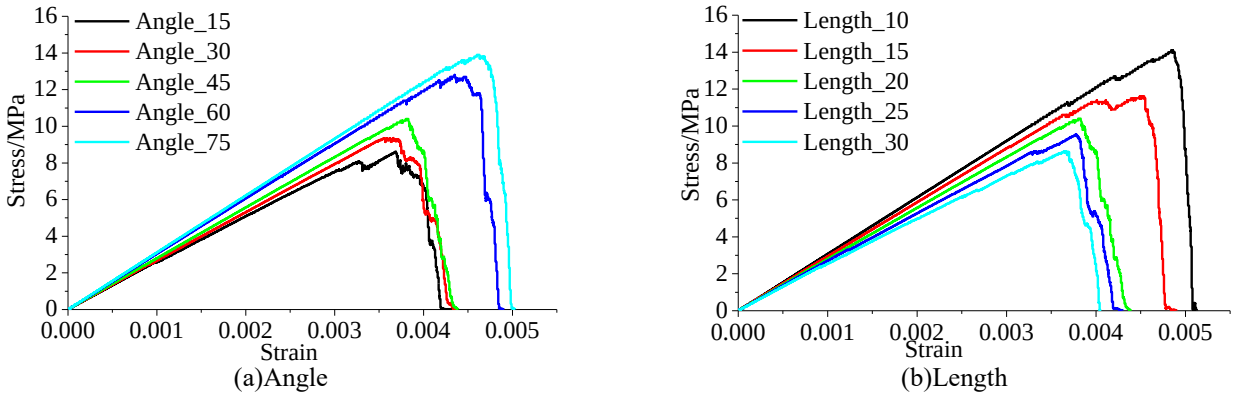

(a)Angle (b)Length

Fig. 8 Stress-strain curves

Table 2 Numerical simulation scheme of different crack characteristics

Scheme	Crack angle/°	Crack length/mm	Crack width/mm
1	15°, 30°, 45°, 60°, 75°	20	1
2	45°	10, 15, 20, 25, 30	1

properties of the composite structure. At the same time, there are no obvious cracks in the coarse sandstone and mudstone specimens, and there are obvious cracks inside the coal specimens through the CT scan images of the coarse sandstone, coal, and mudstone specimens. Therefore, establishing the rock-coal-rock composite structure with different crack characteristics in the coal specimen is of great significance to analyzing of the rock-coal-rock composite mechanical properties and stability. The numerical simulation models of different crack characteristics are shown in Figs. 6 and 7. The numerical simulation scheme is shown in Table 2.

3. Experiment results

3.1 Mechanical properties

Fig. 8 is the stress-strain curves of the rock-coal-rock composite structure with different crack angles and different crack lengths. The peak stress and elastic modulus of the rock-coal-rock composite structure increase with the increase of the crack angle. When the crack angle increases from 15° to 45°, the peak stress and elastic modulus increase slowly, and the distance between the stress-strain curves are small. When the crack angle increases from 45° to 60°, the peak stress and elastic modulus increase faster, and the distance between the stress-strain curves are larger. When the crack angle increases from 60° to 75°, the peak stress and elastic modulus increase slowly, and the distance between the stress-strain curves decreases. It shows that the rock-coal-rock composite structure's peak stress and elastic modulus are more sensitive when the crack angle changes between 45° and 60°.

The peak stress and elastic modulus of the rock-coal-rock composite structure decrease with the crack length increase. When the crack length increases from 10 mm to 15 mm, the peak stress and elastic modulus decrease slowly, and the distance between the stress-strain curves is small. When the crack length increases from 15 mm to 20 mm, the peak stress and elastic modulus decrease quickly, and the distance between the stress-strain curves is large. When the crack length increases from 20 mm to 30 mm, the peak stress and elastic modulus decrease slowly, and the distance between the stress-strain curves decreases. It shows that the rock-coal-rock composite structure's peak stress and elastic modulus are more sensitive when the crack length is between 15 mm and 20 mm.

Fig. 9 is the peak stress variation curve of the rock-coal-rock composite structure with different crack angles and different crack lengths. It can be seen from the figure that the peak stress of the rock-coal-rock composite structure increases with the increase of the crack angle and decreases with the increase of the crack length. Because the smaller the crack angle is, the greater the component force of the stress perpendicular to the crack is at the crack tip, the easier the crack is to expand, and the lower the peak stress is.

When the crack angle increases from 15° to 45°, the crack angle increases by 1°, the peak stress of the composite structure increases 0.059 MPa. When the crack angle increases from 45° to 75°, the crack angle increases by 1°, the peak stress of the composite structure increases 0.117 MPa. The increase of peak stress is small when the crack angle increases from 15° to 45°, and the increase of peak stress is large when the crack angle increases from 45° to 75°. It indicates that the change of crack angle has a great influence on the peak stress when the crack angle is increased from 45° to 75°.

When the crack length increases from 10 mm to 20 mm, the crack length increases by 1 mm, the peak stress of the composite structure decreases 0.37 MPa. When the crack length increases from 20 mm to 30 mm, the crack length increases by 1 mm, the peak stress of the composite structure decreases 0.177 MPa. The decrease of peak stress is large when the crack length increases from 10 mm to 20 mm, and the decrease of peak stress is small when the crack length increases from 20 mm to 30 mm. It indicates that the change of crack length greatly influences the peak stress when the crack length increases 10 mm to 20 mm.

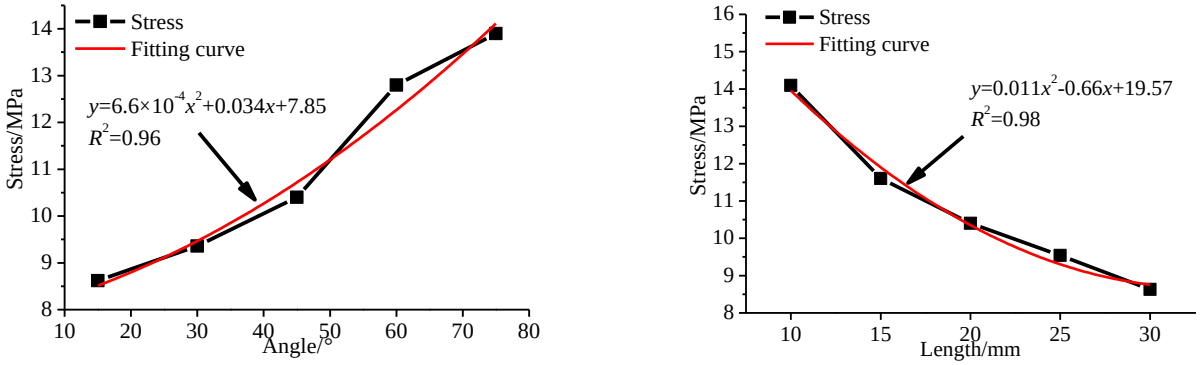

(a) Stress-angle curve (b) Stress-length curve

Fig. 9 Peak stress curves

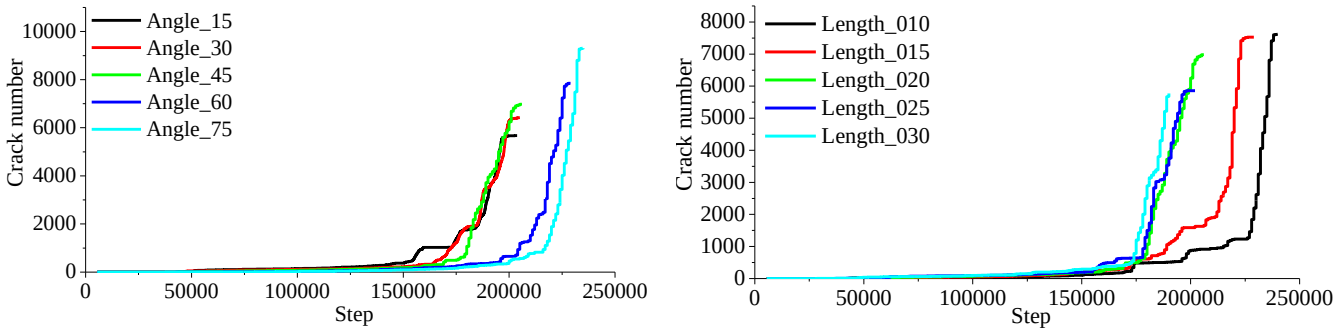

(a) Angle (b) Length

Fig. 10 Crack number curves

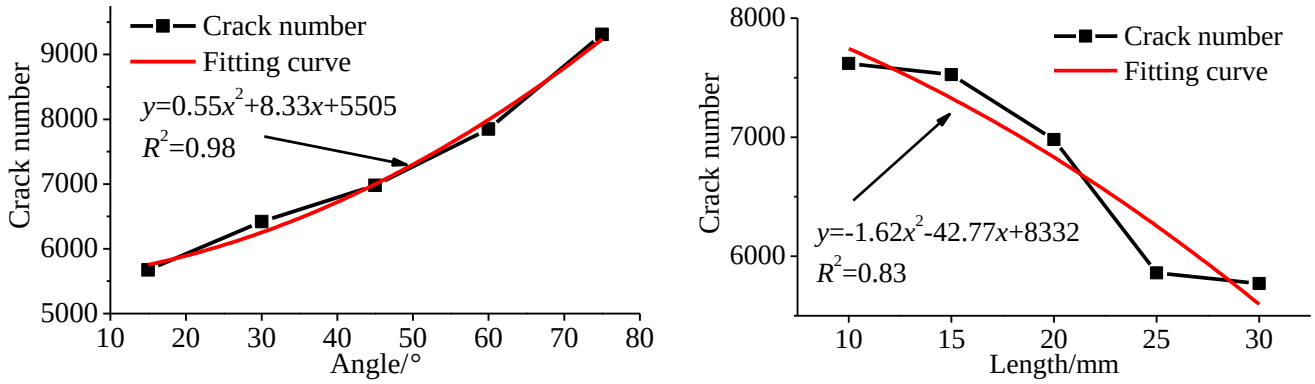

(a) Crack number-angle curve (b) Crack number -length curve

Fig. 11 Maximum crack number curves

The function fitting of crack angle, crack length, and peak stress is carried out, the functional relationship between crack angle and peak stress is as follows

$$y=6.6\times10^{-4}x^2+0.034x+7.85\ (R^2=0.96) \quad (1)$$

The functional relationship between crack length and peak stress is as follows

$$y=0.011x^2-0.66x+19.57\ (R^2=0.983) \quad (2)$$

3.2 Crack propagation

Fig. 10 is the variation curve of the crack number in a rock-coal-rock composite structure with different crack characteristics. As can be seen from the figure, the development and expansion of crack can be divided into three stages:

(1) In The first stage, the pores and cracks in the rock specimen are gradually compacted, and no new cracks are produced.

(2) In The second stage, the fracture gradually expanded. The small cracks are first produced at the tip of pre-existing cracks, and new micro cracks begin to appear in the weak parts of rock specimens, which develop and propagate along the direction parallel to the stress. The crack number increases gradually at this stage.

(3) In The third stage, the crack is connected. With the continuous increase of axial stress, macroscopic cracks

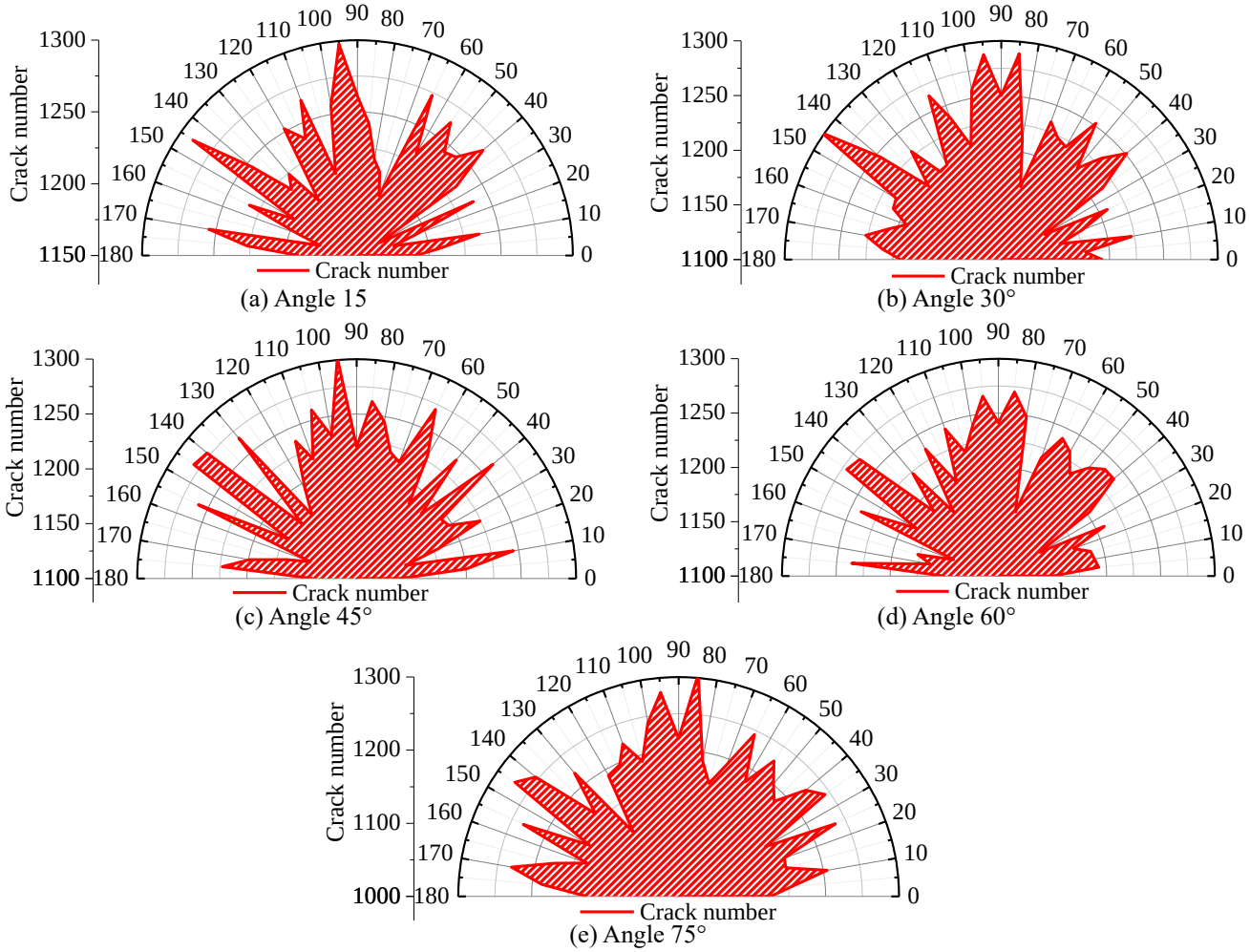

Fig. 12 Rose diagram of the number distribution of new cracks

continue to expand and penetrate, accompanied by rock spatter, rock wall bulge, sheet slope. The crack number

$$y=0.55x^2+8.33x+5505 \ (R^2=0.98) \quad (3)$$

shows a step-by-step growth at this stage.

$$y=-1.62x^2-42.77x+8332 \ (R^2=0.83) \quad (4)$$

Fig. 11 is the variation curve of the maximum crack number. It can be seen from the figure that the maximum crack number in rock-coal-rock composite structure increases with the increase of crack angle and decreases with the increase of crack length.

When the crack angle increase from 15° to 45°, the crack number increased by 1306, accounting for 35.92% of the total increase. When the crack angle increase from 45 ° to 75 °, the crack number increased by 2330, accounting for 64.08% of the total increase. It indicates that the change of crack angle has a great influence on the total crack number when the crack angle increase from 45° to 75°.

When the crack length increase from 10 mm to 15 mm, the crack number decreased by 94, accounting for 5.08% of the total decrease. When the crack length increase from 15 mm to 30 mm, the crack number decreased by 1667, accounting for 90.11% of the total decrease. It indicates that the change of crack length greatly influences the total crack number when the crack length increases from 15 mm to 30 mm.

The function fitting of crack angle, crack length, and the crack number is carried out, the functional relationship between crack angle and the crack number is as follows

The functional relationship between crack length and the crack number is as follows

Fig. 12 is a rose diagram of the number distribution of new cracks in the rock-coal-rock composite structure with different crack angles. When the crack angle is 15°, the newly produced cracks are mainly distributed in the directions of 40°~ 65°, 95 °and 145°. When the crack angle is 30 °, the newly produced cracks are mainly distributed in the directions of 40°~70°, 85°~95°and 145° When the crack angle is 45 °, the newly produced cracks are mainly distributed in the directions of 65°, 85°~95°and 145°. When the crack angle is 60°, the newly produced cracks are mainly distributed in the directions of 40°~65°, 85°~95°and 140°~145°. When the crack angle is 75°, the newly produced cracks are mainly distributed in the directions of 65°, 85°~95°and 140°~145°.

Fig. 13 is the rose diagram of the number distribution of

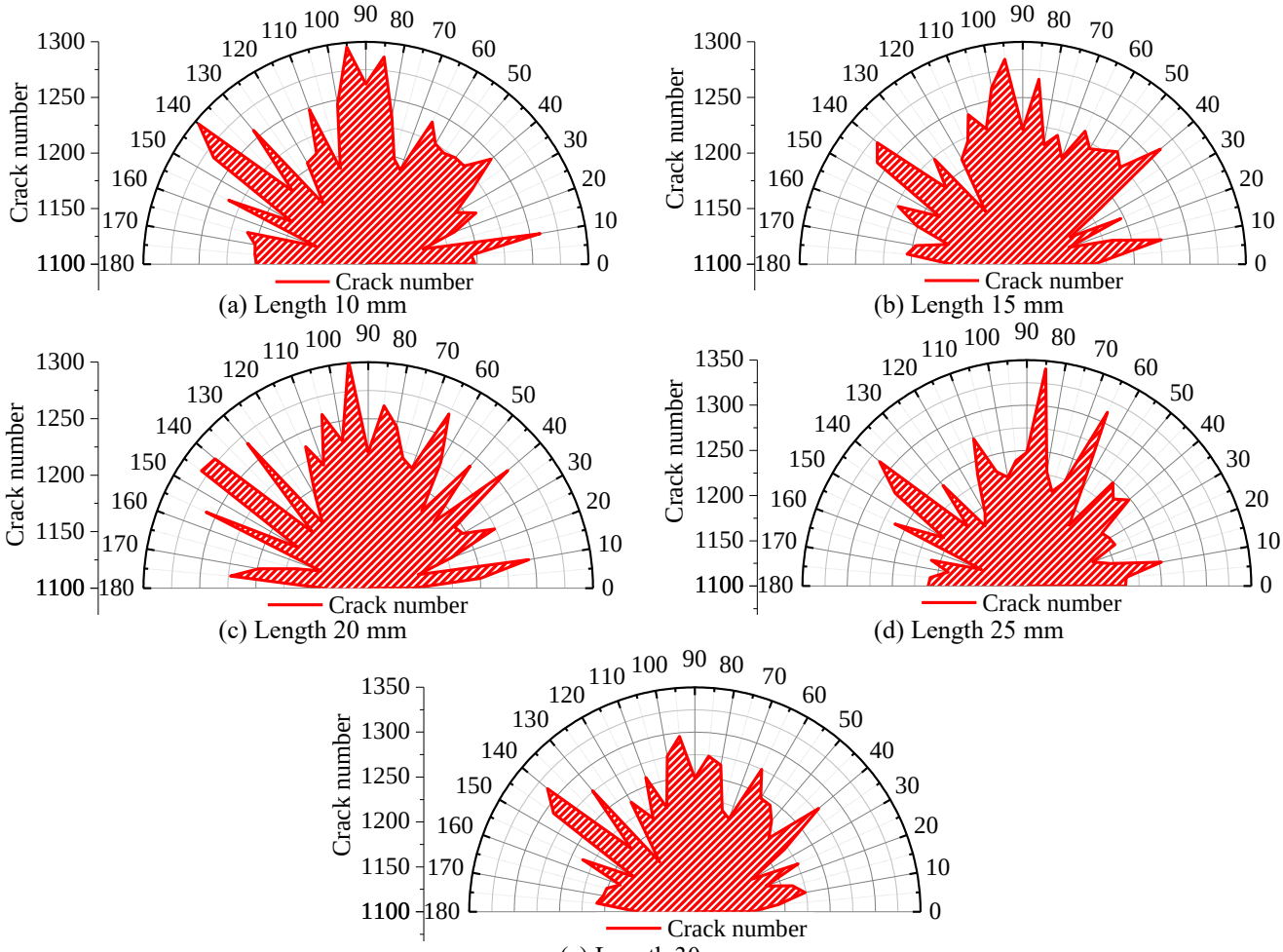

Fig.13 Rose diagram of the number distribution of new cracks

new cracks in the composite structure with different crack lengths. When the crack angle is 10 mm, the newly produced cracks are mainly distributed in the directions of 40°~ 65°, 85°~95°and 140°. When the crack angle is 15 mm, the newly produced cracks are mainly distributed in the directions of 40°, 85°~95°and 140°~145°. When the crack angle is 20 mm, the newly produced cracks are mainly distributed in the directions of 65°, 95°and140°~145°. When the crack angle is 25 mm, the newly produced cracks are mainly distributed in the directions of 65°, 85°and 140°. When the crack angle is 30 mm, the newly produced cracks are mainly distributed in the directions of 40°, 95°and 140°~145°.

Through comparative analysis, it can be seen that the crack number in rock-coal-rock composite structures with different crack characteristics are mainly concentrated in three directions: 45°~ 65°, 85°~ 95°and 140°~ 145°. Among them, the number of newly produced cracks is the largest in the direction of 85°~ 95°.

3.3 Failure characteristics

Figs. 14 and 15 is the failure pattern of rock-coal-rock composite structures with different crack characteristics. It can be seen that the failure of rock- coal-rock composite structure mainly presents splitting failure. The damage degree of the coal specimen is the greatest, accompanied by the ejection of the coal lump. The cracks in coarse sandstone and mudstone specimens are vertical, which is consistent with the stress direction. A large crack zone will be formed in the process of crack formation. When the crack accumulates to a certain extent, one or more large penetrating cracks will cause the failure of the specimen, and these larger penetrating cracks are the main control cracks. The main control crack plays an important role in the stability of the rock-coal-rock composite structure.

Fig. 14 is the failure modes of rock-coal-rock composite structures with different crack angles. The smaller the crack angle is, the more main control cracks are in the coarse sandstone and mudstone specimens, and there are more branch cracks near the main control cracks.

When the crack angle is 15°, the angle between the crack and the newly produced main control crack is 101°. When the crack angle is 75°, the angle between the crack and the newly produced main control crack is 52°. The smaller the crack angle, the larger the angle between the crack and the newly produced main control crack. The larger the crack angle, the smaller the angle between the crack and the newly produced main control crack.

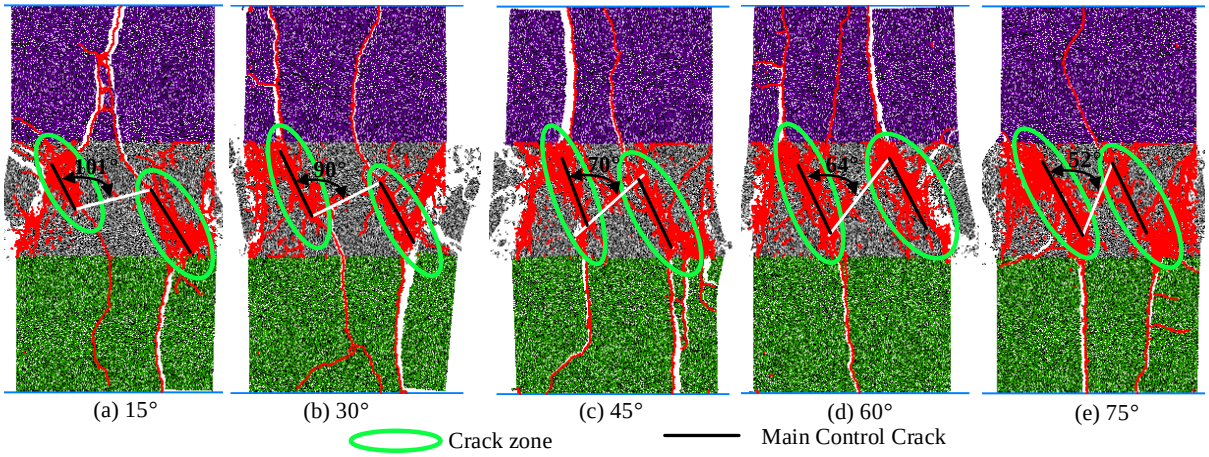

Fig.14 Failure modes of rock-coal-rock composite structures with different crack angles

with the increase of crack angle. When the crack angle

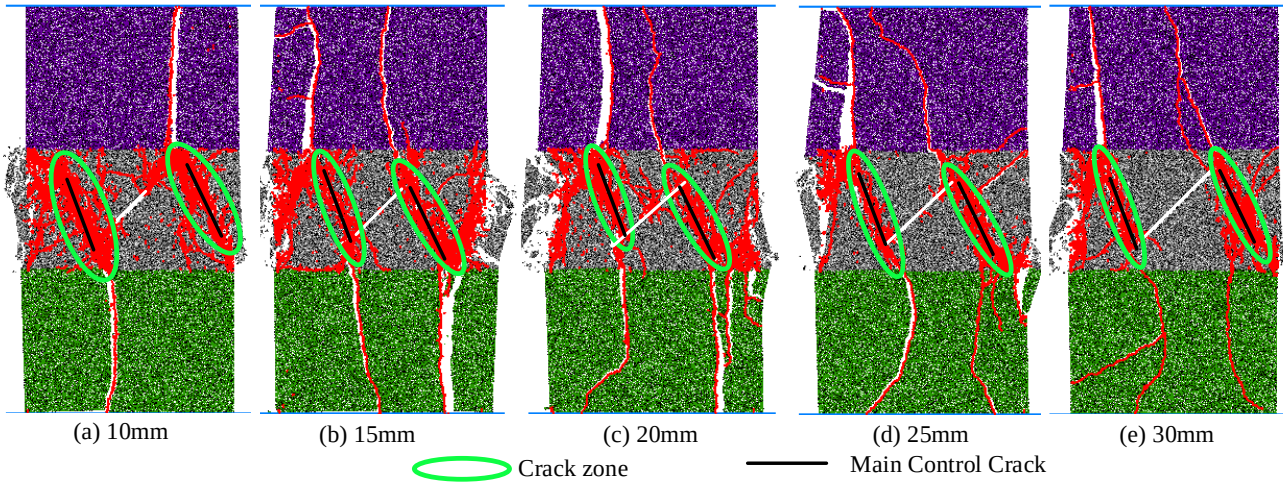

Fig.15 Failure modes of rock-coal-rock composite structures with different crack lengths

Fig. 15 is the failure modes of rock-coal-rock composite structures with different crack lengths. When the crack length is 10 mm, one main control cracks in both the coarse sandstone and mudstone specimens, the main control cracks in the coarse sandstone and mudstone specimens increase with the crack length increase, and there are more branches cracks near the main control cracks. The smaller the crack length, the larger the width of the crack zone. The longer the crack length, the smaller the width of the crack zone.

4. Energy evolution characteristics

The rock is accompanied by the input, accumulation, dissipation, and release of energy from deformation to failure. Analyzing the deformation and failure of rock-coal-rock from the perspective of energy can better discover the essential internal problems of rock-coal-rock instability (Li *et al.* 2017, Zhang *et al*. 2014, Griffith *et al.* 2014, Zhao *et al*. 2010).

Fig. 16 is the energy variation curve of rock-coal-rock composite structures with different fracture characteristics. It can be seen from Fig. 16(a) that the total energy and pre-peak energy of rock-coal-rock composite structure increase increases from 15°to 45°, the pre-peak energy and total energy increase by 0.0039 KJ and 0.0033 KJ, accounting for 23.28% and 19.92% of the total increase, respectively. When the crack angle increases from 45°to 75°, the pre-peak energy and total energy increase by 0.0127 KJ and 0.0134 KJ, accounting for 76.72% and 80.08% total increase, respectively. It indicates that the change of crack angle has a great influence on the pre-peak energy and total energy when the crack angle increases from 45°to 75°. The post-peak energy of a rock-coal-rock composite structure is lower when the prefabricated crack angle is 45°. Because the angle between the crack and the stress is the largest when the crack angle is 45°, the stress decreases rapidly after the composite structure reaches the stress peak, which minimizes the area surrounded by the stress curve and the X-axis.

It can be seen from Fig. 16(b) that the total energy and pre-peak energy of rock-coal-rock composite structure decrease with the increase of fracture length. When the crack length increases from 10 mm to 20 mm, the pre-peak energy and total energy decrease by 0.0157 KJ and 0.0145 KJ, accounting for 81.36% and 75.21% of the total decrease. When the crack length increases from 20 mm to 30 mm, the pre-peak energy and total energy decrease

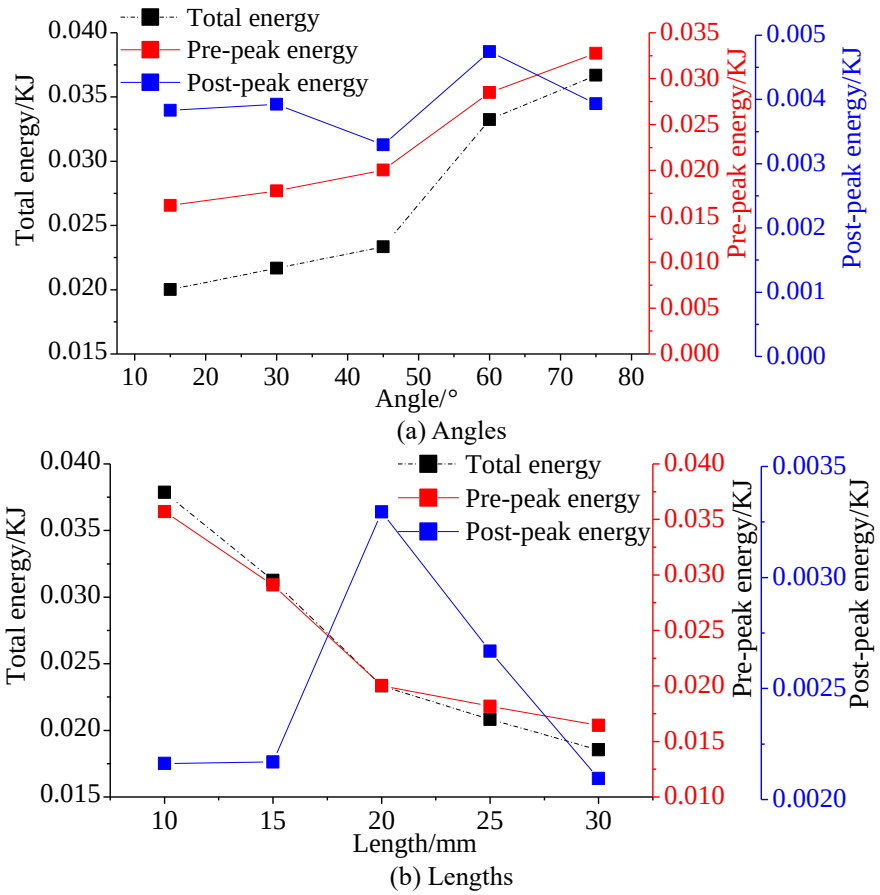

Fig. 16 Energy evolution characteristics

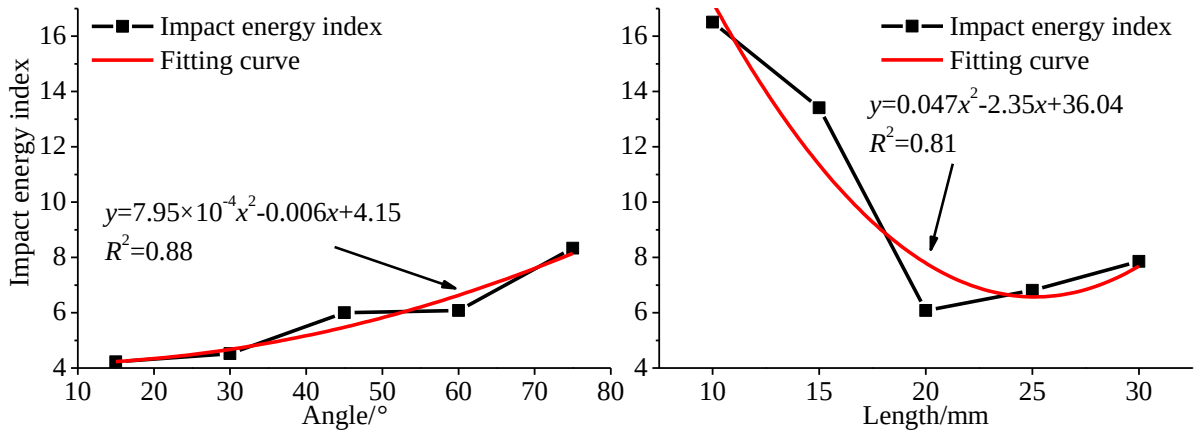

Fig. 17 Impact energy index

0.0036 KJ and 0.0048KJ, accounting for 18.64% and 24.79% of the total decrease, respectively. It indicates that the change of crack length greatly influences the pre-peak energy and total energy when the crack length increases from 10 mm to 20 mm. The post-peak energy increases at first and then decreases with the increase of crack length. When the crack length is 20 mm, the post-peak energy of the rock-coal-rock composite structure reaches the maximum.

The impact energy index is a kind of inherent property of rock mass. The impact energy index is the ratio of accumulated energy before the peak to dissipated energy after the peak, which is expressed by K_e (Sun *et al.* 2019, Li *et al.* 2011). The impact energy index directly and comprehensively reflects the whole process of accumulating and dissipate energy and shows the physical essence of the impact tendency (Kopacz *et al.* 2017, Halim *et al.* 2013). The study of different crack characteristics is of great significance to the stability and impact risk of the rock-coal-rock composite structure.

Fig. 17 is the variation curve of impact energy index of rock-coal-rock composite structure with different crack

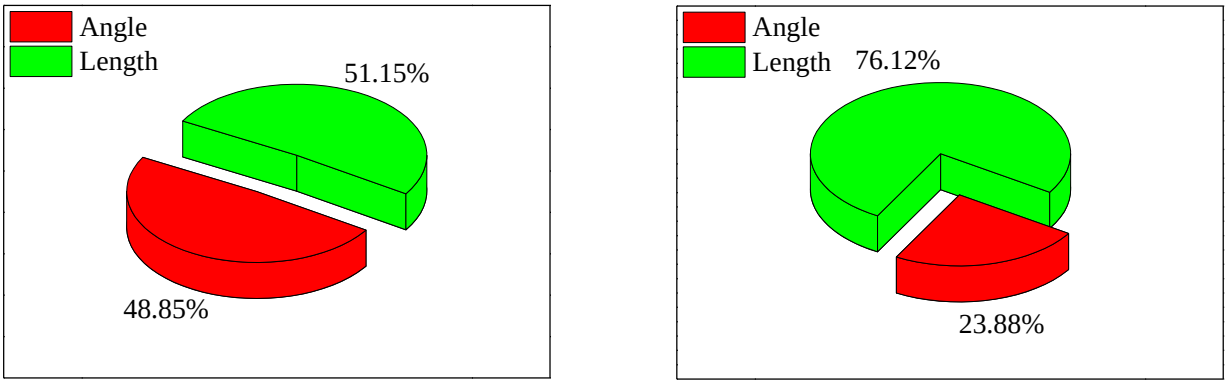

(a) Peak stress (b) Impact energy index

Fig. 18 Sensitivity percentage

characteristics. The impact energy index of the rock-coal-rock composite structure increases with the increase of crack angle. Because the larger the crack angle is, the smaller the angle between the crack and stress is, and the crack deflects to the inside of the composite structure, the tension of the crack outward along the horizontal direction is large, and the impact accident is easy to occur.

The impact energy index of the rock-coal-rock composite structure decreases at first and then increases with crack length. When the crack length is 20 mm, and the crack angle is 45°, the impact energy index of the rock-coal-rock composite structure is the lowest, and the risk of impact is the lowest.

The function fitting of crack angle, crack length, and impact energy index is carried out, the functional relationship between crack angle and impact energy index is as follows

$$y=7.95\times10^{-4}x^2-0.006x+4.15\ (R^2=0.88) \tag{5}$$

The function relationship between crack length and impact energy index is as follows

$$y=0.047x^2-2.35x+36.04\ (R^2=0.81) \tag{6}$$

5. Sensitivity analysis

Based on the above analysis, the functional relationship Z between the crack angle, crack length, and peak stress can be determined, and the functional relationship Y between the crack angle, crack length, and the impact energy index can be determined.

Then

$$Z=a\,f(m)+b\,f(n) \tag{7}$$

$$Y=c\,g(m)+d\,g(n) \tag{8}$$

Where $f(n)$ and $f(m)$ are functions of crack angle, crack length, and peak stress, respectively; a. b is the influence coefficient of crack angle and crack length on the peak stress, $a + b = 1$. $g(n)$ and $g(m)$ are functions of crack angle, crack length and impact energy index respectively; c. c is the influence coefficient of crack angle and crack length on the impact energy index, $c + d = 1$.

Sensitivity analysis is a quantitative method to analyze the influence of the input factors of the model on the target value. Sensitivity analysis can find out the sensitive factors of the model and then increase the control of sensitive factors to achieve the desired goal (Saltelli *et al*. 2010, Filgueira *et al*. 2017).

The basic idea of sensitivity analysis is to fit the analytical expression $z=g(x_1, x_2, x_3, \ldots, x_n)$ between a response function Z and the basic variables$(x_1, x_2, x_3, \ldots, x_n)$ through a finite number of experiments to replace the actual response function $Z=G(x_1, x_2, x_3, \ldots, x_n)$ which can not be expressed clearly. There are two main forms of a response function expression (Hu *et al.* 2021).

The quadratic polynomial response function is

$$g(x)=a+\sum_{i=1}^{n} b_i x_i+\sum_{i\neq j}^{n} c_j x_j^2 \tag{9}$$

Where, $x_i(i=1, 2, 3, \ldots, n)$ is the design variable, a, b_i, $c_j(i, j=1, 2, 3, \ldots, n)$ is an undetermined factor.

The purpose of sensitivity analysis is to understand the sensitivity of the target value to the variation of design parameters. Therefore, this paper uses the dimensionless sensitive factors in system analysis to sort the influencing factors, to distinguish the main parameters and secondary parameters (Patil *et al*. 2020, Castillo *et al*. 2003, Yu *et al.* 2016).

The expression of the sensitivity factor is

$$S_{x_i}=\left|\frac{dg(x)}{dx}\right|\frac{x_i^*}{g(x_i)^*}\quad (i=1,2,\ldots n) \tag{10}$$

Where: S_{x_i} is the sensitive factor when parameter x_i takes the reference value x_i^*; $g(x)$ is the index function of parameter x_i; $g(x_i)^*$ is the index value when parameter x_i takes the reference value x_i^*.

Therefore, the sensitivity percentage γ_{xi} of a design parameter x_i can be expressed as

$$\gamma_{x_i}=\left|\frac{S_{x_i}}{\sum_{i=1}^{n} S_{x_i}}\right| \tag{11}$$

According to the sensitivity analysis, the sensitivity percentage of crack angle and crack length to peak stress and impact energy index is shown in Fig. 18. The sensitive

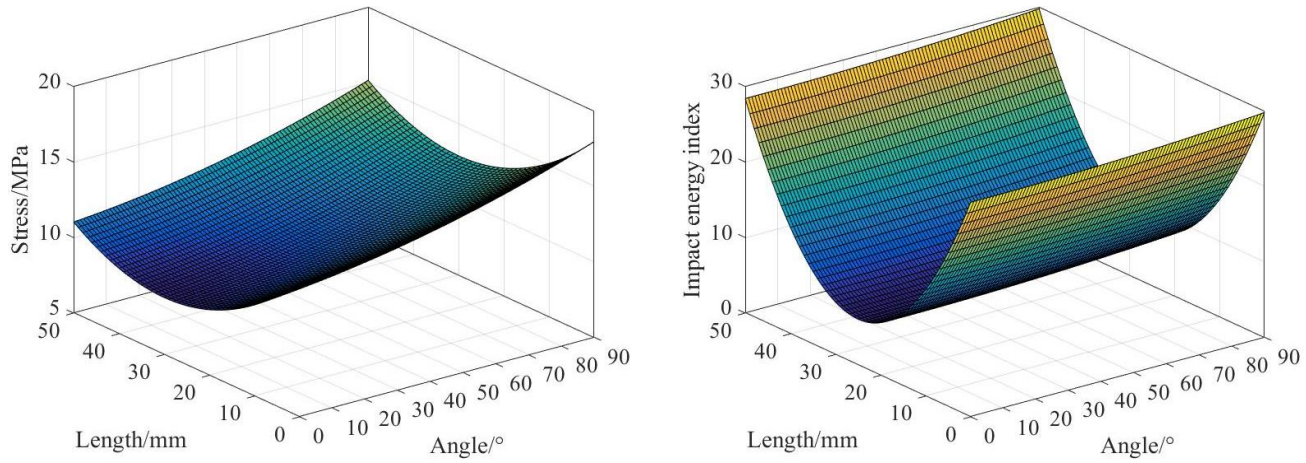

(a) Peak stress (b) Impact energy index

Fig. 19 The three-dimensional surface of the crack characteristics on the stress and impact energy index

percentages of crack angle and crack length to peak stress are 48.85% and 51.15%, respectively. The sensitive percentages of crack angle and crack length to impact energy index are 23.88% and 76.12%, respectively.

Therefore, the functional relationship Z between crack angle, crack length and peak stress can be expressed as follows

$$Z=af(m)+bf(n)=0.4885\,f(m)+0.5115\,f(n)$$
$$=0.4885\,(6.6\times10^{-4}m^2+0.034m+7.85)+0.5115(0.011n^2-0.66n+19.57) \quad (12)$$

The functional relationship Z between crack angle, crack length and impact energy index can be expressed as follows

$$Y=cg(m)+dg(n)=0.2388\,g(m)+0.7612\,g(n)$$
$$=0.2388\,(7.95\times10^{-4}m^2-0.006m+4.15)+0.7612\,(0.047n^2-2.35n+36.04) \quad (13)$$

Where m is the crack angle and n is the crack length.

The functional relationship between crack characteristics and peak stress and impact energy index can make up for the deficiency of the test and comprehensively grasp the influence of crack angle and crack length on peak stress and impact energy index. According to the function of crack angle and crack length with peak stress and impact energy index, the three-dimensional surface is drawn, as shown in Fig. 19. It can be seen from Fig. 19(a) that when the crack length is constant, the peak stress increases gradually with the increase of the crack angle. When the crack angle is constant, the peak stress decreases at first and then increases with the crack length increase, and the peak stress reaches the lowest when the crack length is 30 mm, which is 8.63 MPa. It can be seen from Fig. 19(b) that when the crack length is constant, the impact energy index increases with the increase of the crack angle. When the crack angle is constant, the impact energy index decreases at first and then increases with the crack length increase, and the impact energy index reaches the lowest when the crack length is 20 mm. Therefore, the functional relationship between crack characteristics and peak stress and impact energy index can comprehensively grasp the influence of crack characteristics on peak stress and impact energy index of the rock-coal-rock composite structure.

6. Conclusions

- The peak stress and elastic modulus of rock-coal-rock composite structure increase with the increase of crack angle and decrease with the increase of crack length. When the crack angle increases from 45°to 75°, the crack angle change greatly influences the peak stress. When the crack length increases from 10 mm to 20 mm, the change of crack length greatly influences the peak stress.
- The smaller the crack angle is, the more main control cracks in the coarse sandstone and mudstone specimens, and there are more branch cracks near the main control cracks, and the greater the angle between the new generated main control cracks and cracks. The smaller the crack length is, the larger the width of the crack zone.
- The total energy and pre-peak energy of rock-coal-rock composite structure increase with the increase of crack angle and decrease with the increase of crack length. The post-peak energy increases at first and then decreases with the increase of crack length. When the crack length is 20 mm, the post-peak energy of the rock-coal-rock composite structure reaches the maximum.
- The impact energy index of rock-coal-rock composite structure increases with the increase of crack angle, and decreases at first, and then increases with the increase of crack length. When the crack length is 20 mm, and the crack angle is 45°, the impact energy index of the rock-coal-rock composite structure is the lowest, and the risk of impact is the lowest.
- Using the sensitivity analysis, the functional relationship Z between the crank angle and the crack length, peak stress, and functional relationship Y between the crack and crack lengths and the impact energy index is determined. The determination of the functional relationship makes up for the lack of the relationship between the crack characteristics and the peak stress and impact energy index in the test and fully grasps the influence of the crack angle and the crack length on the peak stress and impact energy index.

Conflicts of interest

The authors declare that there are no conflicts of interests regarding the publication of this paper.

Data availability statement

The authors declare that all data supporting the findings of this study are available within the article. The reader can find and use it, there is no unavailable date.

Acknowledgments

This study was supported by the National Natural Science Foundation of China [grant numbers 51604164]; and the program of youth teacher growth plan in Shandong province.

References

Antonio, B. and Haitao, Y. (2015), "Stress field near the tip of a crack in a poroelastic transversely anisotropic saturated rock", *Eng. Fract. Mech.*, 1411-1418. https://doi.org/10.1016/j.engfracmech.2015.05.006

Bai, J.B., Shen, W.L., Guo, G.L., Wang, X.Y. and Yu, Y. (2015), "Roof deformation, failure characteristics, and preventive techniq-ues of gob-side entry driving heading adjacent to the advancing working face", *Rock Mech. Rock Eng.*, **48**(6), 2447-2458. https://doi.org/10.1007/s00603-015-0713-2.

Castillo, E., Conejo, A.J., Mínguez, R. and Castillo, C. (2003), "An alternative approach for addressing the failure probability-safety factor method with sensitivity analysis", *Reliab. Eng. Syst. Saf.*, **82**(2), 207-216. https://doi.org/10.1016/S0951-8320(03)00164-9.

Chen, S.J., Ge, Y., Yin, D.W. and Yang, H.S. (2019), "An experimental study of the uniaxial failure behaviour of rock-coal composite samples with pre-existing cracks in the coal", *Adv. Civil Eng.*, **2019**(12), 1-12. https://doi.org/10.1155/2019/8397598.

Dehghan, M. and Mohammadi, V. (2016), "The numerical simulation of the phase field crystal (PFC) and modified phase field crystal (MPFC) models via global and local meshless methods", *Comput. Method. Appl. Mech. Eng.*, **298**, 453-484. https://doi.org/10.1016/j.cma.2015.09.018.

Dou, L.M., Lu, C.P., Mu, Z.L., Zhang, X.T. and Li, Z.H. (2006), "Rock burst tendency of coal-rock combinations sample", *J. Min. Saf. Eng.*, **23**(1), 43-46.

Filgueira, U.C., Alejano, L.R., Arzúa, J. and Ivars, D.M. (2017), "Sensitivity analysis of the micro-parameters used in a PFC analysis towards the mechanical properties of rocks", *Procedia Eng.*, **191**, 488-495. https://doi.org/10.1016/j.proeng.2017.05.208.

Filgueira, U.C., Alejano, L.R., Arzúa, J. and Ivars, D.M. (2017), "Sensitivity analysis of the micro-parameters used in a PFC analysis towards the mechanical properties of rocks", *Procedia Eng.*, **191**, 488-495. https://doi.org/10.1016/j.proeng.2017.05.208.

Frith, R. and Reed, G. (2018), "Coal pillar design when considered a reinforcement problem rather than a suspension problem", *Int. J. Min. Sci. Technol.*, **28**(1), 11-19. https://doi.org/10.1016/j.ijmst.2017.11.013.

Griffith, W.A., Becker, J., Cione, K., Miller, T. and Pan, E. (2014), "3D topographic stress perturbations and implications for ground control in underground coal mines", *Int. J. Rock Mech. Min. Sci.*, **70**, 59-68. https://doi.org/10.1016/j.ijrmms.2014.03.013.

Hadjigeorgiou, J., Esmaieli, K. and Grenon, M. (2008), "Stability analysis of vertical excavations in hard rock by integrating a fracture system into a PFC model", *Tunnelling and Underground Space Technology incorporating Trenchless Technology Research*, **24**(3), 296-308. https://doi.org/10.1016/j.tust.2008.10.002.

Halim, M.A., Majumder, R.K., Zaman, M.N. and Hossain, S. (2013), "Mobility and impact of trace metals in barapukuria coal mining area, northwest Bangladesh", *Arabian J. Geosci.*, **6**(12), 4593-4605. https://doi.org/10.1007/s12517-012-0769-1.

Hu, Z.Q., Ma, B., Chen, X.Z. and Tangchirapat, W.C. (2021), "Study on sensitivity parameters analysis of grouting reinforcement underpassing existing subway tunnel by numerical modeling", *Adv. Civil Eng.*, **2021**. https://doi.org/10.1155/2021/8868216.

Jiang, Y.D., Wang, T., Song, Y.M., Wang, X. and Zhang, W. (2013), "Experimental study on the stick-slip process of coal-rock composite samples", *J. China Coal Soc.*, **38**(2), 177-182. https://doi.org/10.13225/j.cnki.jccs.2013.02.013.

Kamran, P., Aliakbar, G. and Takato, T. (2015), "Rock failure assessment based on crack density and anisotropy index variations during triaxial loading tests", *Geomech. Eng.*, **9**(6), 793-813. https://doi.org/10.12989/gae.2015.9.6.793.

Kopacz, M., Kryzia, D. and Kryzia, K. (2017), "Assessment of sustainable development of hard coal mining industry in poland with use of bootstrap sampling and copula-based monte carlo simulation", *J. Cleaner Production*, **159**(15), 359-373. https://doi.org/10.1016/j.jclepro.2017.05.038.

Kurlenya, M.V. and Mirenkov, V.E. (2018), "Deformation of ponderable rock mass in the vicinity of a finite straight-line crack", *J. Min. Sci.*, **54**(6), 893-898. https://doi.org/10.1134/S1062739118065035.

Li, B.F., Liang, X.H. and Qi, L.W. (2011), "Research on the influence of coal's uniaxial compressive strength to impact energy index", *Procedia Eng.*, **26**, 863-868. https://doi.org/10.1016/j.proeng.2011.11.2248.

Li, D.Y., Sun, Z. and Xie, T. (2017), "Energy evolution characteristics of hard rock during triaxial failure with different loading and unloading paths", *Eng. Geol.*, **228**, 270-281. https://doi.org/10.1016/j.enggeo.2017.08.006.

Li, X.S., Liu, Z.F. and Yang, S. (2021), "Similar physical modeling of roof stress and subsidence in room and pillar mining of a gently inclined medium-thick phosphate rock", *Adv. Civil Eng.*, 2021, **17**. https://doi.org/10.1155/2021/6686981.

Li, X.S., Yang, S. and Wang, Y.M. (2021), "Macro-micro response characteristics of surrounding rock and overlying strata towards the transition from open-pit to underground mining", *Geofluids*, 2021, **18**. https://doi.org/10.1155/2021/5582218.

Lisjak, A. and Grasselli, G. (2014), "A review of discrete modeling techniques for fracturing processes in discontinuous rock mass", *J. Rock Mech. Geotech. Eng.*, **6**, 301-314. https://doi.org/10.1016/j.jrmge.2013.12.007.

Liu, W.R., Wang, X. and Li, C.M. (2019), "Numerical Study of Damage Evolution Law of Coal Mine Roadway by Particle Flow Code (PFC) Model", *Geotech. Geol. Eng.*, **37**(4), 2883-2891. https://doi.org/10.1007/s10706-019-00803-6.

Ma, Q., Tan, Y.L., Liu, X.S., Gu, Q.H. and Li, X.B. (2020), "Effect of coal thicknesses on energy evolution characteristics of roof rock-coal-floor rock sandwich composite structure and its damage constitutive model", *Compos. Part B Eng.*, **198**(1), 108086. https://doi.org/10.1016/j.compositesb.2020.108086.

Patil, M.S., Seo, J.H., Panchal, S. and Lee, M.Y. (2020), "Numerical study on sensitivity analysis of factors influencing

liquid cooling with double cold-plate for lithium-ion pouch cell", *Int. J. Energ. Res.*, **45**(2), 2533-2559. https://doi.org/10.1002/ER.5946.

Saltelli, A., Annoni, P., Azzini, I., Campolongo, F. and Tarantola, S. (2010), "Variance based sensitivity analysis of model output. design and estimator for the total sensitivity index", *Comput. Phys. Commun.*, **181**(2), 259-270. https://doi.org/10.1016/j.cpc.2009.09.018.

Sivakumar, G. and Maji, V. B. (2018), "A study on crack initiation and propagation in rock with pre-existing flaw under uniaxial compression", *Indian Geotech. J.*, **48**(4), 626-639. https://doi.org/10.1007/s40098-018-0304-8.

Sun, Z., Li, L., Wang, F. and Zhou, G. (2019), "Desorption characterization of soft and hard coal and its influence on outburst prediction index", *Energy Sources Part A Recovery Utilization and Environmental Effects*, (2), 1-15. https://doi.org/10.1080/15567036.2019.1618991.

Thin, I.G.T., Pine, R.J. and Trueman, R. (1993), "Numerical modelling as an aid to the determination of the stress distribution in the goaf due to longwall coal mining", *Int. J. Rock Mech. Min. Sci*., **30**(7), 1403-1409. https://doi.org/10.1016/0148-9062(93)90128-Z.

Wang, C., Lu, Y., Shen, B., Li, Y. and Liang, Y. (2019), "Design and monitoring of CPB replacement mining RSCP: a case study in China, *Energy Sources, Part A: Recovery*", *Utilization and Environmental Effects*, 80-95. https://doi.org/10.1080/15567036.2019.1623944.

Wang, X.Y., Bai, J.B., Wang, R.F. and Sheng, W.L. (2015), "Bearing characteristics of coal pillars based on modified limit equilibrium theory", *Int. J. Min. Sci. Technol.*, **25**(6), 943-947. https://doi.org/10.1016/j.ijmst.2015.09.010.

Wu, G.S., Yu, W.J., Zuo, J.P. and Du, S.H. (2020), "Experimental and theoretical investigation on mechanisms performance of the rock-coal-bolt(rcb) composite system", *Int. J. Min. Sci. Technol.*, **30**(6), 18-27. https://doi.org/10.1016/j.ijmst.2020.08.002.

Wu, H., Zhang, N., Wang, W.J., Zhao, Y.M. and Cao, P. (2015), "Characteristics of deformation and stress distribution of small coal pillars under leading abutment pressure", *Int. J. Min. Sci. Technol.*, **25**(6), 921-926. https://doi.org/10.1016/j.ijmst.2015.09.007.

Xie, X.Z., Fan, Z.Z., Huang, Z.Z. and Xu, G. (2011), "Research on unsymmetrical loading effect induced by the secondary mining in the coal pillar", *Procedia Eng.*, **26**(26), 725-730. https://doi.org/10.1016/j.proeng.2011.11.2229.

Yang, J.X., Liu, C.Y., Yu, B. and Wu, F.F. (2015), "The effect of a multi-gob, pier-type roof structure on coal pillar load-bearing capacity and stress distribution", *Br. J. Nutr.*, **74**(4), 1267-1273. https://doi.org/10.1007/s10064-014-0685-6.

Yu, L., Wang, S.W., Lu, Q. and Feng, G.H. (2016), "Sensitivity analysis of existing residential building energy consumption influencing factors in cold regions", *Procedia Eng.*, **146**, 196-203. https://doi.org/10.1016/j.proeng.2016.06.372.

Zha, W.H., Shi, H., Liu, S. and Kang, C.H. (2017), "Surrounding rock control of gob-side entry driving with narrow coal pillar and roadway side sealing technology in Yangliu Coal Mine", *Int. J. Min. Sci. Technol.*, **27**(5), 819-823.

Zhang, F., Wang, P., Chen, Z.J. and Xi, A.L. (2014), "Mixture distribution of coal seam thickness and its significance in Zhongji exploration zone of Yulin-Shenmu mining district in northern Shaanxi", *J. Geology*, **2014**.

Zhao, Y.X., Jiang, Y.D. and Tian, S.P. (2010), "Investigation on the characteristics of energy dissipation in the preparation process of coal bumps", *J. China Coal Soc.*, **35**(12), 1979-1983. https://doi.org/10.1016/S1876-3804(11)60004-9.

Zhou, S., Zhu, H.H., Ju, J.W., Yan, Z.G. and Chen, Q. (2017), "Modeling microcapsule-enabled self-healing cementitious composite materials using discrete element method", *Int. J. Damage Mech.*, **26**(2), 340-357. https://doi.org/10.1177/1056789516688835.

Zuo, J.P., Xie, H.P., Wu, A.M. and Liu, J.F. (2011), "Investigation on failure mechanisms and mechanical behaviors of deep coal-rock single body and combined body", *Chinese J. Rock Mech. Eng.*, **30**(1), 84-92. https://doi.org/10.3724/SP.J.1077.2011.00271.

GC